PIV ANALYSIS OF SEDIMENT KINEMATICS IN AN ABUTMENT SCOUR HOLE

ALESSIO RADICE, STEFANO MALAVASI AND FRANCESCO BALLIO

Politecnico di Milano, Dept. I.I.A.R.
Piazza Leonardo da Vinci, 32 – 20133 Milano (Italy)

Velocities (module, angle and direction) of the sediments moving along the bottom surface of an abutment scour hole were calculated by means of a Particle Image Velocimetry technique, after filming the grain motion during a clear water experiment. Grain velocities are relatively stable in time during the first stage of the erosion process, during which scouring is primarily caused by the two-dimensional stream acceleration due to blocking effect of the abutment. Mean grain velocity in front of the obstacle is about one fifth of the mean flow velocity in the unobstructed reach. Erosion at a later stage is driven by the three-dimensional principal vortex and sediment velocity values generally decrease. Velocity module and direction display notable space-time variations, following the alternation of intense transport events due to the flow field action and sediment sliding towards the bottom of the erosion hole.

1 Introduction

Local erosion processes taking place in the vicinity of bridge structures are the result of complex interactions between the flow field due to the obstacle presence and the sediments of the granular bed. These interactions have been generally disregarded by the traditional "black box" experimental approaches, which aim to correlate the maximum erosion depth to the bulk parameters of the incoming flow. On the other hand, many aspects of the phenomenon still lack satisfactory understanding, in spite of the large number of experimental studies on pier and abutment scour that can be found in the literature. Moreover, prediction of the scour depth values under given flow conditions is still linked to many uncertainties, due to the large dispersion of the experimental data (e.g., Radice et al., 2002). These considerations suggest that the description of the erosion process at the small scale can be a useful aid for a better understanding of the phenomenon.

Chang and Yevdjevich (1962) stated that any change in the velocity distribution induced by the presence of the abutment could be responsible for local scour. The majority of experimenters indicated the horseshoe vortex system to be the main scouring agent (see for example Lim, 1993; Melville, 1997; Kothyari and Ranga Raju, 2001; Oliveto and Hager, 2002). This has not been conclusively proved, even though many researches tend to support these ideas. Insight on the matter could be provided by the direct observation of the sediment dynamics at the bottom of the erosion hole, since it is the main consequence of the scouring process. Only a limited number of analysis dealing with clear water scour at bridge structures reported a description of grain motion. Ballio and Orsi (2000) noted that the grain movement is rather regular during the initial stage of

the process, it then becoming unsteady during the advanced stages of scour. Malavasi et al. (2004) specifically analysed the kinematics of the sediments around an abutment at different stages of the scour process. Visualizations of the particle paths allowed identifying the effects of the main scouring agents. Temporal and spatial variability of the grain movement was then analysed by the evaluation of the number of moving particles.

Here we propose a novel application of the Particle Image Velocimetry (PIV) technique to analyse data of Malavasi et al. (2004) related to the motion of grains on the bottom of the scour hole around a bridge abutment.

2 Experiments and PIV analysis

We performed two clear-water laboratory experiments within a rectangular flume, of length $L' = 15$ m, width $W' = 0.60$ m and slope $S = 0.0012$. A layer of nearly uniform sediments ($d_{50} = 1.9$ mm) was placed within the flume. The experiments were performed under the same conditions: water depth was $h = 0.095$ m and mean flow velocity was $U = 0.47$ m/s. The vertical wall abutment had a rectangular shape, of sides $b = 0.20$ m and $L = 0.10$ m, in the transverse and longitudinal directions, respectively (Fig. 1).

During the first run (scour experiment), the erosion depth was measured at various locations in the proximity of the abutment by means of an automatic survey system. Figure 2 depicts the time-evolution of the maximum scour depth d_s. The scour depth displays a well-known trend: while it increases continuously with time T, its rate is a decreasing function of time.

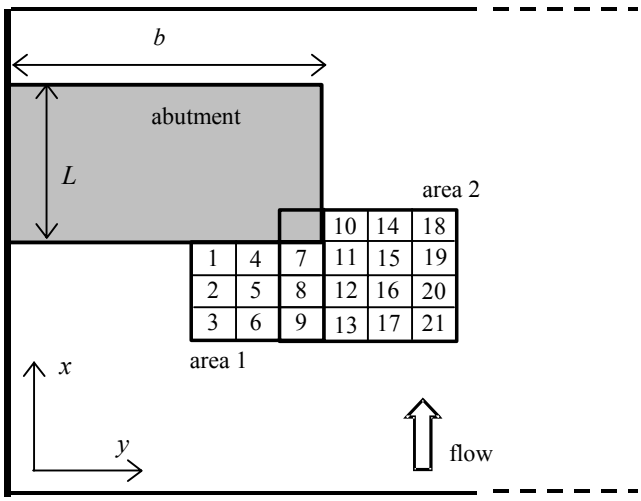

Figure 1. Plan view. The reference coordinate system and the film areas used in the visualization experiment are shown. The subdivision of film areas into inspection windows is also presented.

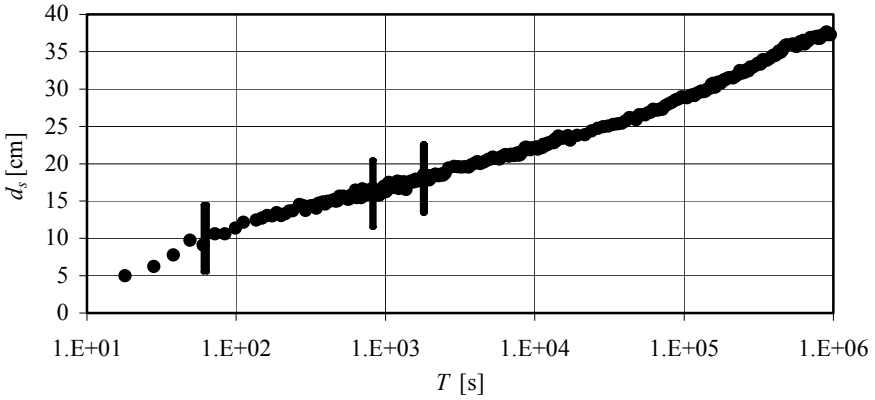

Figure 2. Temporal evolution of the maximum scour depth measured during the scour experiment. The time instants analysed within this work, T_1 = 60 s, T_2 = 810 s, T_3 = 1800 s, are highlighted.

During the second run (visualization experiment), the movement of the sediment was filmed from the top by means of a black and white CCD camera whose resolution and frequency were 576 x 763 pixel and 50 fps, respectively. A wide plexiglass window was placed in the channel to inhibit the water surface. Such a window did not influence the scour depth evolution, as demonstrated by comparing some erosion depth values optically collected during the visualization test and those measured during the scour experiment. The size of the film areas was chosen in order to maintain a good image resolution. The duration of the movies ranged from 2 to 4 seconds. The duration of a single film is negligible with respect to the characteristic times of scour evolution.

Grain velocities were calculated using an ad hoc PIV program. The calculation of a single velocity pattern required three frames of the original movie (herein referred to as F1, F2 and F3). First, the algebraic differences D1 = F2-F1 and D2 = F3-F2 were calculated. Next, D1 and D2 were subdivided into windows of inspection. Each window corresponded to a single location around the abutment. Each location had to be assigned a different velocity value, to take into account the spatial variability of the grain velocity. The size of the windows of inspection was about 3 x 2 cm^2, and was equal to that of Malavasi et al. (2004). Figure 1 shows the subdivision of the film areas. Area 1 and area 2 partially overlap, since windows 7→9 are part of both.

For a given displacement (*dx*, *dy*) an interrogation and a target window could be fitted within the inspection window. Taking all the possible displacements (*dx*, *dy*) smaller than a fixed maximum (equal to one fourth of the size of the inspection window), the most probable movement (*dx*, *dy*) maximizes the parameter:

$$C = \frac{N_x \, N_y}{\sum_{i=1}^{N_x} \sum_{j=1}^{N_y} \left| D_1(i,j) - D_2(i+dx, j+dy) \right|}, \qquad (1)$$

N_x and N_y respectively being the dimensions along x and y of the interrogation and target windows (the adopted coordinate system is reported Figure 1). The velocity components along the x and y directions could then be computed as $u = \underline{dx}/dt$ and $v = \underline{dy}/dt$, dt being the inverse of the frame frequency.

Reliability of the vectors computed was evaluated by calculating the ratio between the maximum and the average values of C. Vectors were eliminated if this ratio was less than 1.1. This typically happened in the presence of small masses of moving sediments and/or small grain velocities. The analysis of the temporal series of velocity components at a single location highlighted the presence of some outliers. These were removed by filtering the signal. The procedure was tested on a set of artificially generated images, obtaining measured velocities within ±15% of the target values.

3 Results

Figure 3 depicts the quadrant analysis of the sediment velocity for area 1 at an initial stage of the process ($T = T_1 = 60$ s). The duration of the movie was 4 seconds. Each plot reports one of the nine locations into which area 1 (upstream of the abutment, see Fig. 1) has been subdivided. Each point on a plot identifies module and direction of a measured velocity vector. With the only exception of a few outliers which have non been automatically removed by the filtering procedure, the experimental points tend to accumulate into well recognizable clouds. The sediment velocity field is relatively stable in time. The instantaneous values can be averaged to obtain the mean velocity field over the length of the film. The pattern obtained by the data of Figure 3 is shown in Figure 4. As suggested by the clouds in Figure 3, all the grain directions are more or less parallel to the upstream face of the abutment, with the exception of those in windows 6 and 9.

This finding is in agreement with the conclusions of Malavasi et al. (2004), who showed that in the initial stage of the scour process the main scouring agent is not the principal vortex, but rather the quasi-steady, two-dimensional acceleration due to the abutment blocking effect. In this phase, the downward and spiraling flow of the principal vortex is stretched along the mean flow direction, and it does not significantly influence the sediment kinematics.

Average velocity in Figures 3 and 4 is about 9 cm/s, corresponding to about one fifth of the mean velocity U of the undisturbed flow. This high value of the sediment velocity during the initial stage of the process is responsible for the large erosion rate that is observed in this phase.

Figure 5 shows the quadrant analysis obtained for area 1 at a more mature stage of scour (time $T = T_3 = 1800$ s). The number of the points in the plot is less than in Figure 3, due to the shorter duration of the film (2 seconds) and to the elimination of a significant number of unreliable vectors (for instance, no reliable vectors were calculated for location 1).

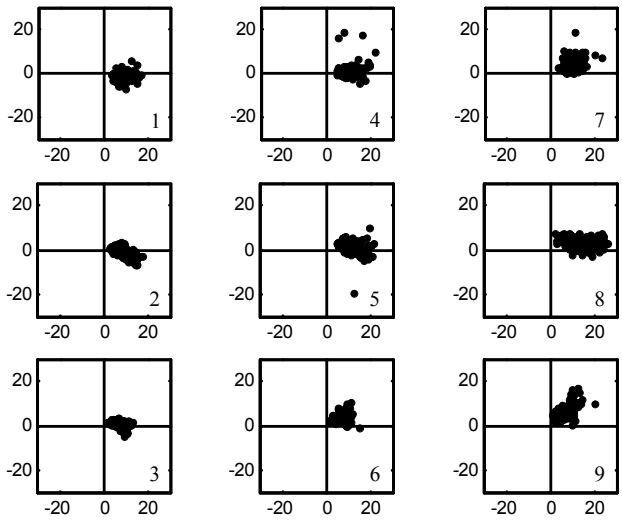

Figure 3. Quadrant analysis of grain velocity for area 1 and time $T = T_1 = 60$ s. The numbering of the locations is indicated for comparison to Fig. 1. On the abscissa axis: v [cm/s]; on the ordinate axis: u [cm/s].

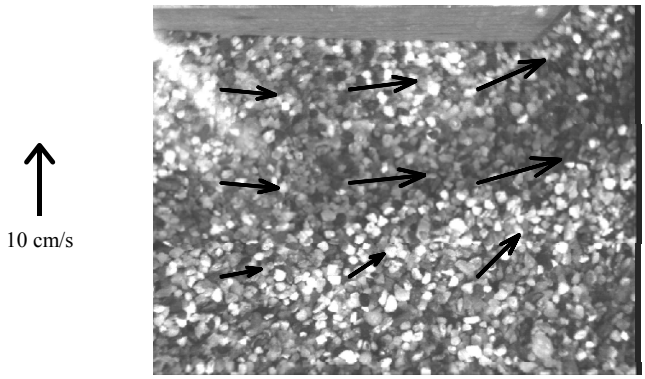

Figure 4. Mean grain velocity field for area 1 and $T = T_1 = 60$ s. Arrow length scale is indicated.

Grain motion shown in Fig. 5 is very different from the one in Fig. 3. Grains are directed away from the abutment during transport events (corresponding to points identifying a negative u component) and they then slide towards the bottom of the hole (points identifying a positive u component). Velocities related to transport events are larger than those related to sliding. The effect of the principal vortex is now recognizable. The vortical flow field becomes the main scouring agent only after a large

enough erosion hole has been created. This behaviour is less evident for locations 2, 4 and 7, where the action of the downflow associated with the principal vortex appears to be weaker, probably because of the presence of the abutment wall.

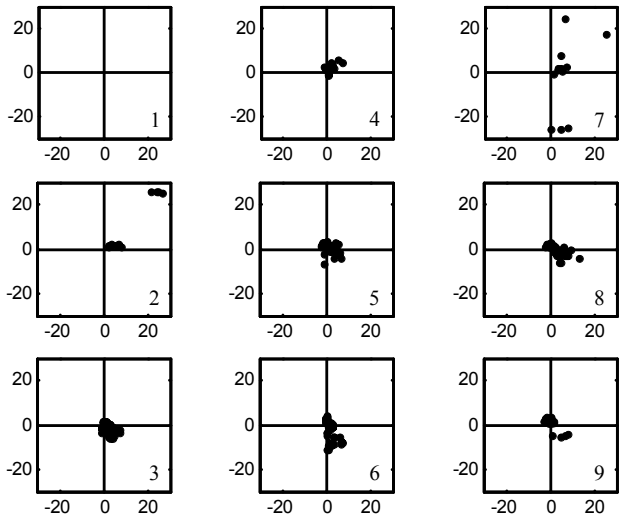

Figure 5. Quadrant analysis of grain velocity for area 1 and time $T = T_3 = 1800$ s. The numbering of the locations is indicated for comparison to Fig. 1. On the abscissa axis: v [cm/s]; on the ordinate axis: u [cm/s].

Figure 6 shows the quadrant analysis of the velocity values for area 2 at a different stage of the process (time $T = T_2 = 810$ s). The film duration was 2 seconds. Locations 7, 8 and 9 are also part of area 1. Comparing the corresponding plots in Figures 5 and 6 allows confirming the phenomenological considerations presented , despite the difference between times T_2 and T_3. The action of the principal vortex is also clearly recognized at the lateral locations (mostly at locations 13, 12, 16, 15 and 14; see Figure 1 for numbering), where the principal directions of movement are somehow radial departing from the abutment nose, in agreement to the spiraling shape of the vortical structure. Again, velocities of sediments displaced by the flow during transport events are considerably larger than velocities of sediments sliding down the hole towards the abutment face. Grain velocities are smaller at locations closer to the abutment wall, where the downflow is weaker.

The mean grain velocity field obtained from the data of Figure 6 is shown in Figure 7. On average, the sediments move towards the centre of the channel, to be finally conveyed downstream along the mean flow direction. Comparison between the arrows length in Figures 7 and 4 shows that mean flow velocity strongly decreases as the phenomenon progresses in time. Despite grain velocities relative to transport events being similar in the initial and in the development stages, the average grain velocity

observed in the development stages is small (about 2.5 cm/s, nearly 5% of the mean undisturbed flow velocity) due to the prevalent presence of two opposite directions. As a consequence, the scour mechanism is comparatively less efficient than that observed in the initial stage of the process.

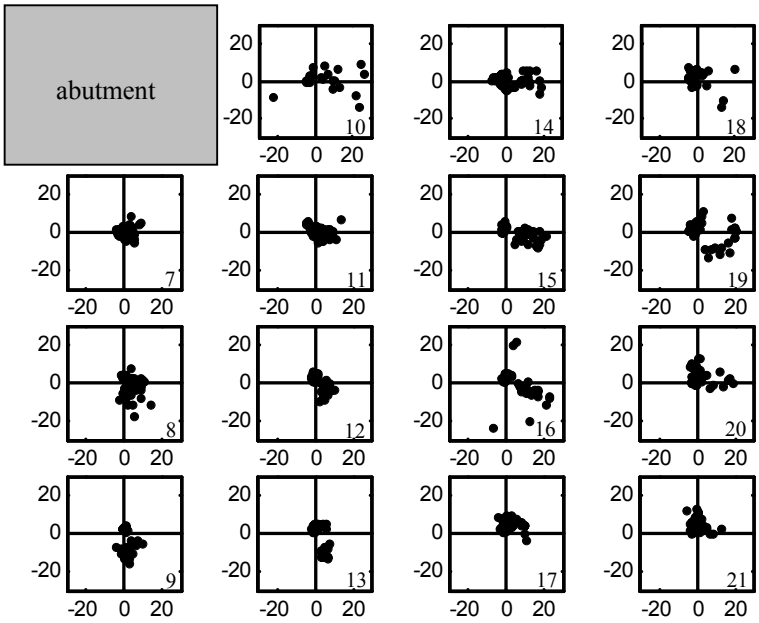

Figure 6. Quadrant analysis of grain velocity for area 2 and time $T = T_2 = 810$ s. The numbering of the locations is indicated for comparison to Fig. 1. On the abscissa axis: v [cm/s]; on the ordinate axis: u [cm/s].

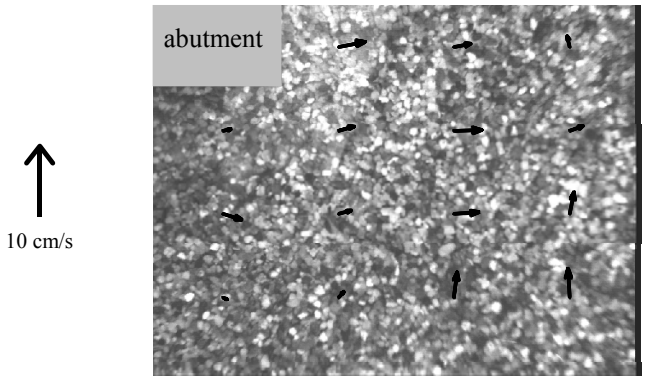

Figure 7. Average grain velocity field for area 2 and time $T = T_2 = 810$ s. Arrow length scale indicated.

4 Conclusions

Velocities of sediments moving along the bottom of a local abutment scour hole have been evaluated by means of a PIV procedure.
In the first part of the phenomenon, erosion is driven by the two-dimensional acceleration at the abutment nose. The average grain velocity in front of the obstacle is about 20% of that of the mean undisturbed flow. The action of the principal vortex system becomes evident only after a large enough erosion hole has been scoured. The velocities of the grains during a transport event are similar to those observed in the initial stage, but transport events are alternate with low velocity sediment sliding towards the bottom of the hole. Mean velocities are small in this phase (about 5% of the mean flow velocity), due to the presence of two opposite main directions. Thus, the scouring mechanism of the initial stage is much more efficient than that observed during the development stage. This is in agreement with the observed temporal decreasing rate of scour depth.

Acknowledgments

The present research has been supported by Italian Minister for Scientific Research under the contracts "Influenza di vorticità e turbolenza nelle interazioni dei corpi idrici con gli elementi al contorno e ripercussioni sulle progettazioni idrauliche" and "Strutture coerenti in fenomeni erosivi localizzati".

References

Ballio, F. and Orsi, E. (2000). “Time evolution of scour around bridge abutments.” *Water Engineering Research*, 2(4), 243-259.

Chang, F.M. and Yevdjevich, V.M. (1962). “Analytical study of local scour.” *Report for the U.S. Dept. of Commerce, Bureau of Public Roads; Univ. of Colorado, Dept. of Civil Engineering*.

Kothyari, U.C. and Ranga Raju, K.G. (2001). “Scour around spur dikes and bridge abutments.” *Journal of Hydraulic Research*, 39(4), 367-374.

Lim, S.Y. (1997). “Equilibrium clear-water scour around an abutment.” *Journal of Hydraulic Engineering*, 123(3), 237-243.

Malavasi, S., Radice, A. and Ballio, F. (2004). “Study of sediment motion in a local scour hole through an image processing technique.” *River Flow 2004, II Int. Conf. on Fluvial Hydraulics, Naples, Italy*, 1, 535-542.

Melville, B.W. (1997). “Pier and abutment scour: integrated approach.” *Journal of Hydraulic Engineering*, 123(2), 125-136.

Oliveto, G. and Hager, W.H. (2002). “Temporal evolution of clear-water pier and abutment scour.” *Journal of Hydraulic Engineering*, 128(9), 811-820.

Radice A., Franzetti S. and Ballio F. (2002). “Local scour at bridge abutments.” *River Flow 2002, I Int. Conf. on Fluvial Hydraulics, Louvain-la-Neuve, Belgium,* 2, 1059-1068.